

Manuscript Number:

Title: The effect on bending waves by defects in pinned elastic plates

Article Type: Full Length Article

Section/Category: F Structural vibration/elastic wave propagation

Keywords: Thin elastic plate, defects, pinned plate, scattering, forcing, periodic array

Corresponding Author: Mr. Michael Smith, Ph. D. student

Corresponding Author's Institution: University of Auckland

First Author: Michael Smith, Ph. D. student

Order of Authors: Michael Smith, Ph. D. student; Richard Porter; Timothy D Williams

Abstract: This paper presents solutions to a number of problems posed for the out-of-plane displacement of infinite thin elastic plates that are rigidly pinned in periodic configurations, but that possess a finite number of 'defects'. We begin by considering a single one-dimensional periodic array of pins. We derive an analytic solution for the displacement produced by the forced oscillation of the central pin in the array, and this solution is shown to be closely connected to the problem of scattering of plane waves by an array when a finite number of pins are removed. Attention then focuses on doubly-periodic rectangular arrays of pinned points possessing defects. Central to approaching such problems is an understanding of Bloch-Floquet waves in periodic arrays in the absence of defects and a simple method is described for computing the associated dispersion surfaces. The solution to three problems are then sought: the trapping of localized waves by a finite number of missing pins; trapping of waves by entire rows of missing pins; and the wave radiation pattern due to the forcing of a single pin.

All problems are treated analytically by using bounded Green's functions for thin elastic plates, a discrete Fourier transform solution method and simple, explicit and rapidly convergent evaluations of the one- and two-dimensional lattice sums that arise.

1 The effect on bending waves by defects in pinned elastic
2 plates

3 Michael J. A. Smith^{a,*}, Richard Porter^b, Timothy D. Williams^c

4 ^a*Department of Mathematics, University of Auckland, Private Bag 92019, Auckland, NZ*

5 ^b*School of Mathematics, University of Bristol, Bristol, BS8 1TW, UK*

6 ^c*Nansen Environmental and Remote Sensing Center, Thormøhlens gate 47, N-5006*
7 *Bergen, Norway*

8 **Abstract**

9 This paper presents solutions to a number of problems posed for the out-
10 of-plane displacement of infinite thin elastic plates that are rigidly pinned
11 in periodic configurations, but that possess a finite number of ‘defects’. We
12 begin by considering a single one-dimensional periodic array of pins. We
13 derive an analytic solution for the displacement produced by the forced
14 oscillation of the central pin in the array, and this solution is shown to
15 be closely connected to the problem of scattering of plane waves by an
16 array when a finite number of pins are removed. Attention then focuses
17 on doubly-periodic rectangular arrays of pinned points possessing defects.
18 Central to approaching such problems is an understanding of Bloch-Floquet
19 waves in periodic arrays in the absence of defects and a simple method is
20 described for computing the associated dispersion surfaces. The solution to
21 three problems are then sought: the trapping of localized waves by a finite
22 number of missing pins; trapping of waves by entire rows of missing pins;
23 and the wave radiation pattern due to the forcing of a single pin.

All problems are treated analytically by using bounded Green’s functions
for thin elastic plates, a discrete Fourier transform solution method and

*

Preprint submitted to Journal of Sound and Vibration *January 17, 2012*
Corresponding author. Contact number: +64 09 373 8768, Fax: +64 09 373 7457

Email addresses: m.smith@math.auckland.ac.nz (Michael J. A. Smith),
richard.porter@bristol.ac.uk (Richard Porter), timothy.williams@nersc.no
(Timothy D. Williams)

simple, explicit and rapidly convergent evaluations of the one- and two-dimensional lattice sums that arise.

24 *Keywords:* Thin elastic plate, defects, pinned plate, scattering, forcing,
25 periodic array.

26 **1. Introduction**

27 Thin elastic plates are used in many engineering applications and are
28 often either bonded to a substructure along ribs or rigidly pinned by rivets.
29 Determining the transmission properties due to defects in the vibrations
30 along periodically ribbed elastic sheets and membranes was the subject of
31 a series of significant papers published over a number of decades [e.g. 1, 2,
32 3, 4, 5]. In these investigations, the elastic membrane or thin elastic plate
33 is viewed in cross-section and bounded above by a two-dimensional acoustic
34 fluid. The interest in such problems lies in how sound waves couple with
35 vibrational modes on a periodically-supported elastic beam. The defects
36 consisted of vibrating ribs and laterally displaced rib supports, the latter
37 giving rise to localization effects [e.g. 6].

38 Evans and Porter [7] [also see 8], motivated in part by the work men-
39 tioned above, considered so-called Very Large Floating Structures in which
40 they imagined a large two-dimensional thin elastic sheet secured to the sea
41 bed by mooring lines that provided periodic point supports on the elastic
42 sheet. In this situation, although the underlying three-dimensional incom-
43 pressible fluid does not support body waves, coupling still exists between
44 the fluid and elastic sheet. Their work highlighted the mathematical ele-
45 gance of using point sources (or Green's functions) to represent the effect
46 of point forces on an elastic sheet. In particular, whilst wave theories such
47 as acoustics, electromagnetics and elasticity are governed by second-order

48 partial differential equations, the Kirchhoff equation for a thin elastic plate
49 is fourth order in space. Consequently, point sources behave like $r^2 \log r$ as
50 the distance r to the source is approached rather than diverging like $\log r$ as
51 in source solutions to second order wave equations. This fact permits source
52 functions to be used as physical representations of small clamped circular
53 pins. We remark that isotropic point sources can be used as an approxi-
54 mate model for acoustic wave scatterers in the limit of small, widely-spaced,
55 soft-sound cylinders and long wavelengths [eg. 9, §8.2.5].

56 A variety of work on two-dimensional thin elastic sheets has followed,
57 mainly choosing to ignore the complication of coupling to an external fluid.
58 For example, Movchan et al. [10] computed the band-gap structure for a
59 doubly periodic arrangement of holes of finite radius with either clamped
60 or free edges. The dispersion relation for Bloch-Floquet waves through a
61 periodically pinned sheet was obtained analytically by taking the limit of
62 a clamped hole radius tending to zero. This particular problem, whose
63 solution also appears in Evans and Porter [8], is revisited in section 3 of
64 the current paper where a simpler approach to computing the band-gap
65 structure is described. Other recent related works on pinned elastic plates
66 include [11, 12, 13] and [14].

67 The focus of the present paper is to examine the effect of introducing
68 ‘defects’ into both one- and two-dimensional infinite periodic arrays of rigidly
69 pinned points in a thin elastic plate. In this paper a defect will mean either
70 removing one or more pins from the array, or replacing a rigid pin by one
71 which is forced to oscillate periodically in time at a prescribed amplitude.
72 The mathematical difficulty in solving defect problems of this type arises as
73 the geometry is no longer periodic.

74 Defects in one-dimensional periodic arrays have been considered in the

75 setting of the two-dimensional Helmholtz equation for a linear array of
76 acoustically-hard or soft cylinders by Thompson and Linton [15]. There
77 the solution is approached using the so-called ‘Modified Array Scanning
78 Method’. Its use of transform methods and excitation of waves by point
79 sources to represent the defects bears similarities to the approach used in the
80 present paper. However, our methods proceed more directly and transpar-
81 ently, evidently due to the simplicity afforded by using single point sources
82 to represent pins. Earlier, Thompson and Linton [16] had used the array
83 scanning method to consider the excitation of an acoustic wave field by a
84 line source in the presence of a periodic array of cylinders.

85 Defects in doubly-periodic arrays are of current interest in several re-
86 search fields including elastodynamics [17], phononic crystals [18] and pho-
87 tonic crystals [19, 20, 21, 22, 23]. Techniques for determining defect modes
88 range from the method of fictitious sources, to supercell methods and multi-
89 pole methods. Attention has also been focused on understanding the effects
90 of defects in more complicated photonic structures such as woodpiles [24].

91 Bloch-Floquet problems occur frequently in many application areas of
92 the physical sciences and central to the understanding of defects in doubly-
93 periodic arrays is the consideration of the associated homogeneous problem
94 without defects. Often they are related to the solution of the wave (or
95 Helmholtz’s) equation which requires the evaluation of lattice sums which
96 in their most basic form are poorly convergent. Hence acceleration of lattice
97 sums for computational purposes is crucial. As a result, efficient methods
98 for the evaluation of convergent lattice sums (using Graf’s addition theorem
99 and integral techniques) for Helmholtz’s equation in a doubly periodic do-
100 main continue to be developed [e.g. 25], Movchan et al. [26] and Chin et al.
101 [27]. Linton [28] provides an exhaustive survey of the most commonly used

102 techniques.

103 In contrast to those methods cited above for Helmholtz's equation, here
104 we are able to derive convergent, readily computable lattice sums for prob-
105 lems posed using the thin elastic plate equation using standard methods
106 without the need to accelerate convergence characteristics. This is evidently
107 a consequence of the low order of the condition applied at pinned points
108 (zero) compared to the order of the governing equation (four). In particu-
109 lar, this means that the Green's function that produces the point sources
110 used to represent the pinned points is bounded everywhere.

111 Our general method of solution is applied first in section 2 to one-
112 dimensional arrays. The roots of this method can be traced to [2] and are
113 based on Fourier transforming the infinite systems of equations that arise
114 from the application of pin conditions. Two distinct problems naturally
115 arise: the wave radiation pattern due to the time-harmonic forcing of the
116 central pin; and the scattering of plane waves by a number of missing pins
117 in an array.

118 Solution methods for linear periodic arrays are then extended to more
119 complicated and arguably more interesting problems involving doubly-periodic
120 arrays of pins, and here we investigate possible localized modes that are sup-
121 ported by defects. In total, three problems are considered here: the effect
122 of removing one or more pins from the plate; the wave radiation pattern
123 due to the forced motion of a single pin; and the effect of removing entire
124 rows of pins. These are presented in section 3, and in section 4, a selection
125 of results are presented from each of the problems considered in the paper.
126 The work is summarised in section 5 where an indication is given to how
127 these methods may be extended to other related and physically interesting

128 problems.

129 **2. Defects in a single periodic array of pinned points**

130 An infinite thin elastic plate occupies the (x', y') plane having an out-
131 of-plane displacement $u'(x', y')$, and is assumed to be pinned rigidly along
132 the line $y' = 0$ at $x = ma'$ for $m \in \mathbb{Z} \setminus \mathcal{M}$ where \mathcal{M} is a finite set which
133 represents points in an otherwise periodic array which are not rigidly pinned
134 (i.e. defects). In the simplest case $\mathcal{M} = \{0\}$ means all but the origin
135 is pinned. The period of the array is represented by a' , and we consider
136 two problems in this section. In the first, $\mathcal{M} = \{0\}$ and in its place, the
137 point $(0, 0)$ is excited by a forcing of amplitude C at angular frequency ω .
138 (This problem shall be referred to as the *forced pin problem*.) In the second
139 problem, a periodic array with defects is excited by an incident plane wave
140 of fixed amplitude and angular frequency ω from infinity, propagating at an
141 angle θ_0 with the negative y' -axis.

142 In both cases, the governing equation for a thin elastic plate is given by

$$(\Delta'^2 - k^4)u' = 0, \quad (1)$$

143 where Δ' is the two-dimensional Laplacian, $k^4 = m\omega^2/D$, $m = \rho h$ is the
144 mass per unit area in terms of the plate thickness h and density ρ . Also,
145 $D = (1/12)Eh^3/(1 - \nu^2)$ is the flexural rigidity defined in terms of Young's
146 modulus E and Poisson's ratio ν . The conditions at the fixed pins is

$$u'(ma', 0) = 0, \quad m \in \mathbb{Z} \setminus \mathcal{M}. \quad (2)$$

147 Non-dimensionalising lengths with respect to k via $x = kx'$, $y = ky'$ and
148 $a = ka'$ with $u(x, y) = u'(x', y')/C$ converts (1) and (2) into

$$(\Delta^2 - 1)u(x, y) = 0, \quad (3)$$

149 and

$$u(ma, 0) = 0, \quad m \in \mathbb{Z} \setminus \mathcal{M}, \quad (4)$$

150 where the parameter $a = ka'$ is the only dimensionless parameter left in this
151 problem.

152 We first consider the problem of pin forcing at the centre of the one-
153 dimensional periodic array. This solution is then used to construct the
154 solution to the scattering of plane waves by a defective array in the following
155 subsection.

156 *2.1. Forcing of the central pin*

157 Here we consider the problem of forcing a single pin with unit amplitude
158 in a periodic linear array of pinned points in the absence of an incident wave
159 field. We use the superscript (f) throughout to distinguish this problem
160 from later problems, and introduce the notation $u_m^{(f)} = u^{(f)}(ma, 0)$, $m \in \mathbb{Z}$,
161 to represent the displacement at the point $x = ma$ in the array. For this
162 problem $\mathcal{M} = \{0\}$ and the pinned conditions $u_m^{(f)} = 0$ are set for $m \notin \mathcal{M}$
163 whilst at the origin $u_0^{(f)} = 1$ is imposed. The total displacement of the plate
164 can be written as

$$u^{(f)}(x, y) = \sum_{n=-\infty}^{\infty} a_n^{(f)} g(x - na, y), \quad (5)$$

165 where $g(x, y)$ represents a Green's function for a source placed at the origin
166 of a thin plate satisfying

$$(\Delta^2 - 1)g(x, y) = \delta(x)\delta(y), \quad (6)$$

167 and given explicitly by

$$g(x, y) = \frac{i}{8} (H_0(r) - H_0(ir)), \quad (7)$$

168 where H_0 represents a Hankel function of the first kind and $r^2 = x^2 + y^2$.

169 Note that at the origin the Green's function is bounded as $g(0, 0) = i/8$.

170 In (5), the coefficients $a_n^{(f)}$ are to be determined. Enforcing the boundary
171 conditions at each point in the array on (5) gives

$$u_m^{(f)} = \sum_{n=-\infty}^{\infty} a_n^{(f)} g((m-n)a, 0) = \delta_{m,0}, \quad (8)$$

172 for all m , where $\delta_{m,n}$ represents the Kronecker delta function. Accordingly,
173 multiplying through by $e^{-im\theta}$ and summing over all m results in

$$1 = \sum_{m=-\infty}^{\infty} \sum_{n=-\infty}^{\infty} a_n^{(f)} g((m-n)a, 0) e^{-im\theta}, \quad (9)$$

174 where θ refers to the standard angular polar coordinate.

175 We now define the following finite Fourier transforms (Fourier series)
176 with

$$A^{(f)}(\theta) = \sum_{n=-\infty}^{\infty} a_n^{(f)} e^{-in\theta}, \quad a_n^{(f)} = \frac{1}{2\pi} \int_{-\pi}^{\pi} A^{(f)}(\theta) e^{in\theta} d\theta \quad (10a)$$

$$G_0(\theta; a) = \sum_{n=-\infty}^{\infty} g(na, 0) e^{-in\theta}, \quad g(na, 0) = \frac{1}{2\pi} \int_{-\pi}^{\pi} G_0(\theta; a) e^{in\theta} d\theta. \quad (10b)$$

177 The series in (10b) has been computed in Evans and Porter [7] and it
178 helps to outline this process here. Thus the integral representations of the
179 Hankel functions allow us to write the Green's function as

$$g(x, y) = \frac{1}{8\pi} \int_{-\infty}^{\infty} \mathcal{G}(t, y) e^{ixt} dt, \quad \mathcal{G}(t, y) = \frac{e^{-\lambda(t)|y|}}{\lambda(t)} - \frac{e^{-\gamma(t)|y|}}{\gamma(t)}, \quad (11)$$

180 where

$$\lambda(t) = \begin{cases} (t^2 - 1)^{1/2}, & |t| \geq 1, \\ -i(1 - t^2)^{1/2}, & |t| < 1, \end{cases} \quad \text{and } \gamma(t) = (1 + t^2)^{1/2}. \quad (12)$$

181 Applying the Poisson summation formula

$$2\pi \sum_{n=-\infty}^{\infty} f(2n\pi) = \sum_{n=-\infty}^{\infty} \int_{-\infty}^{\infty} e^{\pm inu} f(u) du, \quad (13)$$

182 to expression (11) at the points $(x, y) = (na, 0)$ and comparing with (10b)
 183 readily admits the convergent series

$$G_0(\theta; a) = \frac{1}{4a} \sum_{n=-\infty}^{\infty} \mathcal{G}(t_n, 0), \quad (14)$$

184 where $t_n = (\theta + 2n\pi)/a$. It can be shown that the summand $\mathcal{G}(t_n, 0)$ has
 185 a leading order asymptotic behaviour of $a^3/(2\pi|n|)^3$ as $|n| \rightarrow \infty$, so conver-
 186 gence can be accelerated by writing

$$G_0(\theta; a) = \frac{1}{4a} \left(\mathcal{G}(t_0, 0) + \frac{2a^3}{(2\pi)^3} \zeta(3) \right) + \frac{1}{4a} \sum_{n=1}^{\infty} \left(\mathcal{G}(t_n, 0) + \mathcal{G}(t_{-n}, 0) - \frac{2a^3}{(2n\pi)^3} \right), \quad (15)$$

187 where ζ denotes the Riemann zeta function. This forces (15) to converge
 188 like $O(|n|^{-5})$. It can also be seen that G_0 is both symmetric and periodic:

$$G_0(-\theta; a) = G_0(\theta; a), \quad G_0(\theta + 2m\pi; a) = G_0(\theta; a) \quad \text{for } m \in \mathbb{Z}. \quad (16)$$

189 The definitions above allow expression (9) for the forcing of a single pin to
 190 be written in the form

$$1 = A^{(f)}(\theta) G_0(\theta; a), \quad (17)$$

191 after using the convolution result for Fourier series. Rearranging (17) for
 192 $A^{(f)}(\theta)$ and inverting from (10a) admits

$$a_n^{(f)} = \frac{1}{2\pi} \int_{-\pi}^{\pi} \frac{e^{in\theta}}{G_0(\theta; a)} d\theta. \quad (18)$$

193 It is proved in Evans and Porter [7] that $G_0(\theta; a)$ does not vanish, and
 194 this postpones the complications associated with singularities in integrals
 195 that we encounter in later parts of the paper.

196 As a corollary to the above solution, we can see from (8) that

$$\begin{aligned} \sum_{n=-\infty}^{\infty} a_{n-r}^{(f)} g((m-n)a, 0) &= \sum_{n'=-\infty}^{\infty} a_{n'}^{(f)} g((m-r-n')a, 0) \\ &= \delta_{m-r,0} = \delta_{m,r}. \end{aligned} \quad (19)$$

197 Therefore, once the coefficients $a_n^{(f)}$ have been determined from the problem
198 of forcing a pin at the origin, the coefficients needed for forcing the r^{th} pin
199 are just $a_{n-r}^{(f)}$.

200 In the far-field, in terms of polar coordinates (ρ, χ) centred on the ori-
201 gin, we can substitute the large argument asymptotic form of the Green's
202 function from (6) into (5) to give

$$u^{(f)}(x, y) \sim \frac{i}{8} \sum_{n=-\infty}^{\infty} a_n^{(f)} \left(\frac{2}{\pi\rho} \right)^{1/2} e^{i(\rho - na \cos \chi)} e^{-i\pi/4}, \quad (20)$$

203 as $\rho \rightarrow \infty$. Alternatively we could say

$$u^{(f)}(x, y) \sim \left(\frac{2}{\pi\rho} \right)^{1/2} e^{i\rho - i\pi/4} \mathcal{A}^{(f)}(\chi), \quad (21)$$

204 where

$$\mathcal{A}^{(f)}(\chi) = \frac{i}{8} \sum_{n=-\infty}^{\infty} a_n^{(f)} e^{-ina \cos \chi} \equiv \frac{i}{8} A^{(f)}(a \cos \chi), \quad (22)$$

205 is the usual diffraction coefficient.

206 2.2. Scattering of plane waves by defects in a 1D periodic array

207 We now move on to considering plane wave scattering by a linear periodic
208 array of pinned points containing a finite number of missing pins, encoded
209 in the set \mathcal{M} . The superscript (s) is used to denote quantities associated
210 with this scattering problem. Here, we let $u_m^{(s)} = u^{(s)}(ma, 0)$ for all m and
211 so $u_m^{(s)} = 0$ for $m \in \mathbb{Z} \setminus \mathcal{M}$. The total displacement is written as

$$u^{(s)}(x, y) = u^{(i)}(x, y) + \sum_{n=-\infty}^{\infty} a_n^{(s)} g(x - na, y), \quad (23)$$

212 where the prescribed incident wave plate displacement is given by

$$u^{(i)}(x, y) = e^{i\alpha_0 x + \lambda(\alpha_0) y}, \quad (24)$$

213 with $\alpha_0 = \sin \theta_0$ and $\lambda(\alpha_0) = -i \cos \theta_0$ is defined in (12).

214 In expression (23), the coefficients $a_n^{(s)}$, $n \notin \mathcal{M}$ are to be determined,
 215 whilst we set $a_n^{(s)} = 0$ for $n \in \mathcal{M}$ since there is no contribution to the
 216 scattered field from pins that are removed from the array. Enforcing the
 217 pinned conditions on the general solution (23) gives

$$0 = u^{(i)}(ma, 0) + \sum_{n=-\infty}^{\infty} a_n^{(s)} g((m-n)a, 0), \quad m \notin \mathcal{M}. \quad (25)$$

218 Note that for $m \in \mathcal{M}$, the left hand side of the above expression is replaced
 219 with the unknown displacement at each of the removed pins,

$$u_m^{(s)} = u^{(i)}(ma, 0) + \sum_{n=-\infty}^{\infty} a_n^{(s)} g((m-n)a, 0), \quad m \in \mathcal{M}. \quad (26)$$

220 Equations (25) and (26) can consequently be combined and written in the
 221 suggestive form

$$\sum_{r \in \mathcal{M}} u_r^{(s)} \delta_{m,r} = u^{(i)}(ma, 0) + \sum_{n=-\infty}^{\infty} a_n^{(s)} g((m-n)a, 0), \quad m \in \mathbb{Z}. \quad (27)$$

222 The structure of (27) allows a solution to be written as a superposition of the
 223 separate effects of incident wave scattering by an unbroken periodic array
 224 and forcing of strength $u_r^{(s)}$ at each of locations $r \in \mathcal{M}$ in the absence of an
 225 incident wave. In other words,

$$a_n^{(s)} = a_n^{(u)} + \sum_{r \in \mathcal{M}} u_r^{(s)} a_{n-r}^{(f)}, \quad (28)$$

226 following use of the forcing solution (19), the coefficients $a_n^{(f)}$ having previ-
 227 ously been determined by (18), whilst $a_n^{(u)}$ is the solution of

$$-u^{(i)}(ma, 0) \equiv -e^{im\alpha_0 a} = \sum_{n=-\infty}^{\infty} a_n^{(u)} g((m-n)a, 0), \quad m \in \mathbb{Z}, \quad (29)$$

228 which is the equation for the scattering by an uninterrupted grating. The
 229 periodicity of the left-hand side of (29) implies a periodicity of the solution,
 230 so $a_n^{(u)} = a_0^{(u)} e^{in\alpha_0 a}$. Using this in (29) gives

$$-1 = a_0^{(u)} \sum_{n=-\infty}^{\infty} g(-na, 0) e^{in\alpha_0 a} = a_0^{(u)} G_0(-\alpha_0 a; a) = a_0^{(u)} G_0(\alpha_0 a; a), \quad (30)$$

231 using (10b) and (16), and so the final form of (28) is

$$a_n^{(s)} = -\frac{e^{in\alpha_0 a}}{G_0(\alpha_0 a; a)} + \sum_{r \in \mathcal{M}} u_r^{(s)} a_{n-r}^{(f)}. \quad (31)$$

232 The remaining unknowns, $u_r^{(s)}$ for $r \in \mathcal{M}$, are determined by imposing the
 233 remaining condition $a_n^{(s)} = 0$ for $n \in \mathcal{M}$ in (31) resulting in the linear system

$$\frac{e^{in\alpha_0 a}}{G_0(\alpha_0 a; a)} = \sum_{r \in \mathcal{M}} u_r^{(s)} a_{n-r}^{(f)}, \quad n \in \mathcal{M}. \quad (32)$$

234 When a single pin at the origin is missing, that is $\mathcal{M} = \{0\}$, the solution of
 235 (31), (32) is given explicitly by

$$a_n^{(s)} = \frac{1}{G_0(\alpha_0 a; a)} \left(-e^{in\alpha_0 a} + \frac{a_n^{(f)}}{a_0^{(f)}} \right). \quad (33)$$

236 In the scattering problem, there are two components to the far-field: plane
 237 waves reflected by an uninterrupted periodic pin grating and circular waves
 238 emanating from the defects. In the case of a single missing pin at the origin,
 239 these circular waves are easily identified from the second term in (33) to be
 240 related to those for the forcing problem so that the diffraction coefficient for
 241 the circular wave component of the scattered field is simply

$$\mathcal{A}^{(s)}(\chi) = \frac{\mathcal{A}^{(f)}(\chi)}{a_0^{(f)} G_0(\alpha_0 a; a)}, \quad (34)$$

242 with $\mathcal{A}^{(f)}$ defined by (22). More generally, for multiple missing pins, the
 243 contribution from the sum in (31) to far-field circular waves results in a

244 diffraction coefficient given by

$$\begin{aligned} \mathcal{A}^{(s)}(\chi) &= \frac{i}{8} \sum_{n=-\infty}^{\infty} \sum_{r \in \mathcal{M}} u_r^{(s)} a_{n-r}^{(f)} e^{-ina \cos \chi} \\ &= \mathcal{A}^{(f)}(\chi) \sum_{r \in \mathcal{M}} u_r^{(s)} e^{-ira \cos \chi}. \end{aligned} \quad (35)$$

245 The first term in the right-hand of either (31) or (33) accounts for the
246 diffracted wave field from an unbroken periodic array and its contribution
247 to the total displacement may be written as

$$u^{(u)}(x, y) = -\frac{1}{G_0(\alpha_0 a; a)} \sum_{n=-\infty}^{\infty} e^{in\alpha_0 a} g(x - na, y). \quad (36)$$

248 Using the definition (11) in the above and invoking Poisson's summation
249 formula gives

$$u^{(u)}(x, y) = \frac{-1}{4aG_0(\alpha_0 a; a)} \sum_{n=-\infty}^{\infty} e^{i\alpha_n x} \left(\frac{e^{-\lambda(\alpha_n)|y|}}{\lambda(\alpha_n)} - \frac{e^{-\gamma(\alpha_n)|y|}}{\gamma(\alpha_n)} \right), \quad (37)$$

250 where

$$\alpha_n = \alpha_0 + 2n\pi/a. \quad (38)$$

251 We can define scattering angles, θ_n , defined by $\alpha_n = \sin \theta_n$, which extend the
252 definition of $\alpha_0 = \sin \theta_0$ introduced for the incident wave. Then, providing
253 $|\alpha_n| < 1$, θ_n are real angles corresponding to propagating waves and we say
254 that $n \in \mathcal{N}$. (\mathcal{N} is non-empty as it always contains the zero element.) For
255 such values of n , $\lambda(\alpha_n) = -i \cos \theta_n$, allowing (37) to be written as

$$u^{(u)}(x, y) \sim \frac{-1}{4aG_0(\alpha_0 a; a)} \sum_{n \in \mathcal{N}} \frac{e^{ix \sin \theta_n} e^{i|y| \cos \theta_n}}{(-i \cos \theta_n)} \quad (39)$$

256 as $|y| \rightarrow \pm\infty$. In $y > 0$, (39) represents reflected plane waves propagating
257 away from the array (located at $y = 0$) at scattering angles θ_n with ampli-
258 tudes $R_n = -i/(4aG_0(\alpha_0 a; a) \cos \theta_n)$ whilst in $y < 0$, the superposition of the
259 incident wave field implies transmitted wave amplitudes of $T_n = \delta_{n,0} + R_n$.
260 These are well-known effects in diffraction grating theory [7].

261 **3. Defects in a doubly-periodic array of pinned points**

262 We now move on to consider problems involving doubly-periodic arrays
 263 of pinned points. Specifically, we choose to pin an infinite elastic plate at
 264 the points $(x, y) = (na, mb)$ for $(n, m) \in \mathbb{Z}_2 \setminus \mathcal{M}$, where a and b denote the
 265 periodicity of the rectangular lattice in the two perpendicular directions on
 266 the plate. The set \mathcal{M} represents lattice indices where defects occur, i.e.
 267 where pins are missing. In the simplest case of a single defect at the origin,
 268 $\mathcal{M} = \{(0, 0)\}$. There are two problems we can consider here. The first
 269 problem is one in which the origin is forced to oscillate with a set frequency
 270 and unit amplitude. The interest here lies in how the radiated wave energy
 271 may escape through the lattice to infinity as a function of angular frequency,
 272 ω . The second is the possibility of locating trapped modes in the vicinity of
 273 the defect(s) in the lattice. These are localized wave motions which oscillate
 274 indefinitely and do not radiate energy away to infinity within the otherwise
 275 periodic lattice of pinned points.

276 As we shall show, both problems require information about Bloch-Floquet
 277 waves in an infinite doubly-periodic lattice without defects, which will ap-
 278 pear as a byproduct of our analysis.

279 *3.1. Forcing of the central pin*

280 Let us again consider the forcing problem first, as the defect problem can
 281 (as shown in §2) be written as a superposition of solutions to the forcing
 282 problems over the set of defects. A general solution is written as

$$u^{(f)}(x, y) = \sum_{n=-\infty}^{\infty} \sum_{m=-\infty}^{\infty} a_{n,m}^{(f)} g(x - na, y - mb), \quad (40)$$

283 where we impose pinned conditions $u_{n,m}^{(f)} \equiv u^{(f)}(na, mb) = 0$, $(n, m) \notin \mathcal{M}$,
 284 where $\mathcal{M} = \{(0, 0)\}$. At the origin we set $u_{0,0}^{(f)} = 1$ to represent the forcing.

285 Applying these conditions to (40) gives

$$\delta_{p,0}\delta_{q,0} = \sum_{n=-\infty}^{\infty} \sum_{m=-\infty}^{\infty} a_{n,m}^{(f)} g((p-n)a, (q-m)b), \quad (41)$$

286 for all $p, q \in \mathbb{Z}$. Multiplying this through by $e^{-ip\theta}e^{-iq\phi}$ and summing over
287 all p and q results in

$$1 = \sum_{p=-\infty}^{\infty} \sum_{q=-\infty}^{\infty} \sum_{n=-\infty}^{\infty} \sum_{m=-\infty}^{\infty} a_{n,m}^{(f)} g((p-n)a, (q-m)b) e^{-ip\theta} e^{-iq\phi}. \quad (42)$$

288 Using the convolution result for Fourier series and rearranging, this can be
289 expressed as

$$1 = A^{(f)}(\theta, \phi) G(\theta, \phi; a, b), \quad (43)$$

290 where

$$A^{(f)}(\theta, \phi) = \sum_{n=-\infty}^{\infty} \sum_{m=-\infty}^{\infty} a_{n,m}^{(f)} e^{-in\theta} e^{-im\phi}, \quad (44)$$

291 and

$$G(\theta, \phi; a, b) = \sum_{n=-\infty}^{\infty} \sum_{m=-\infty}^{\infty} g(na, mb) e^{-in\theta} e^{-im\phi}, \quad (45)$$

292 whilst the inversion formula associated with (44) is

$$a_{n,m}^{(f)} = \frac{1}{4\pi^2} \int_{-\pi}^{\pi} \int_{-\pi}^{\pi} A^{(f)}(\theta, \phi) e^{in\theta} e^{im\phi} d\theta d\phi. \quad (46)$$

293 The equation (45) defining $G(\theta, \phi; a, b)$ is a double lattice sum and in the
294 present form is not suitable for computation as the series is very slowly
295 convergent. We follow the procedure already used for a single periodic array
296 to convert (45) into a more convergent series. Thus, we use the integral
297 representation (11) in (45) to give

$$G(\theta, \phi; a, b) = \frac{1}{8\pi} \sum_{m=-\infty}^{\infty} \sum_{n=-\infty}^{\infty} \int_{-\infty}^{\infty} \mathcal{G}(t, mb) e^{in(at-\theta)-im\phi} dt. \quad (47)$$

298 Using Poisson's summation formula for the n summation gives

$$G(\theta, \phi; a, b) = \frac{1}{4a} \sum_{m=-\infty}^{\infty} \sum_{n=-\infty}^{\infty} \left(\frac{e^{-\lambda(t_n)|m|b}}{\lambda(t_n)} - \frac{e^{-\gamma(t_n)|m|b}}{\gamma(t_n)} \right) e^{-im\phi}, \quad (48)$$

299 where $t_n = (\theta + 2n\pi)/a$ again. Then, reversing the order of summation
 300 in (48) and summing the resulting geometric series for m gives, after some
 301 routine algebra,

$$G(\theta, \phi; a, b) = \frac{1}{4a} \sum_{n=-\infty}^{\infty} \left(\frac{1}{\lambda(t_n)} \frac{\sinh(\lambda(t_n)b)}{\cosh(\lambda(t_n)b) - \cos \phi} - \frac{1}{\gamma(t_n)} \frac{\sinh(\gamma(t_n)b)}{\cosh(\gamma(t_n)b) - \cos \phi} \right), \quad (49)$$

302 which is now absolutely convergent. We observe that

$$G(\theta + 2p\pi, \phi + 2q\pi; a, b) = G(\theta, \phi; a, b) \quad \text{for } p, q \in \mathbb{Z}, \quad (50a)$$

$$G(\theta, \phi; a, b) = G(\theta, -\phi; a, b) = G(-\theta, \pm\phi; a, b), \quad (50b)$$

303 and also that G is real-valued. Returning to (43), and inverting the trans-
 304 form using (46) gives

$$a_{n,m}^{(f)} = \frac{1}{4\pi^2} \int_{-\pi}^{\pi} \int_{-\pi}^{\pi} \frac{e^{in\theta} e^{im\phi}}{G(\theta, \phi; a, b)} d\theta d\phi \quad (51)$$

305 In contrast to section 2, in which coefficients were defined in terms of
 306 a single integral with a denominator G_0 which is strictly positive, in (51)
 307 there is the possibility that G will vanish along curves in the two-dimensional
 308 domain of integration.

309 We therefore consider the implication of vanishing G . A reworking of
 310 (42) and (43) in the case of a doubly-periodic array without any defects
 311 results in homogeneous versions of those equations and hence non-trivial
 312 solutions are found when

$$G(\theta, \phi; a, b) = 0. \quad (52)$$

313 The resulting solutions have the quasi-periodicity property in that the ex-
 314 pansion coefficients $a_{m,n}^{(b)}$ used in place of $a_{m,n}^{(f)}$ in (40), satisfy the relation

$$a_{m,n}^{(b)} = a_{0,0}^{(b)} e^{in\theta} e^{im\phi} = a_{0,0}^{(b)} e^{i\mathbf{r}_{n,m} \cdot \boldsymbol{\alpha}}$$

315 where $\mathbf{r}_{n,m} \equiv (na, mb)$ are position vectors of pins in the array, $\boldsymbol{\alpha} = (\alpha, \beta)$
 316 is the Bloch wave vector and $\theta \equiv \alpha a$, $\phi \equiv \beta b$. Such solutions represent
 317 Bloch-Floquet waves (hence the superscript (b)). It helps to make full use
 318 of this change of coordinates to define

$$\tilde{G}(\boldsymbol{\alpha}; a, b) = G(\theta, \phi; a, b) \quad (53)$$

319 defined on $-\pi/a \leq \alpha \leq \pi/a$ and $-\pi/b \leq \beta \leq \pi/b$, the fundamental cell
 320 of the reciprocal lattice. Solutions of (52) form propagation surfaces in
 321 (α, β, a) -space which depend on the lattice aspect ratio b/a . Assuming the
 322 aspect ratio b/a and dimensionless frequency a to be fixed, \tilde{G} vanishes along
 323 the curves of constant frequency on the propagation surfaces satisfying $\tilde{G} =$
 324 0 . If $\tilde{G} \neq 0$ throughout the fundamental cell of the reciprocal lattice then the
 325 frequency a is said to lie in a stop-band; wave propagation is impossible in all
 326 directions. Otherwise the frequency is said to lie in a pass band and waves
 327 can propagate throughout the infinite array. The permissible directions
 328 of wave propagation are *not* defined by the direction of the Bloch wave
 329 vector (α, β) along the curves of constant frequency, but in the direction
 330 of $\nabla \tilde{G} \equiv (\tilde{G}_\alpha, \tilde{G}_\beta)$ evaluated along those curves. This is because energy
 331 propagates in the direction of the group velocity vector, and not in the
 332 direction of the phase vector [29].

333 We rewrite (51) as

$$a_{n,m}^{(f)} = \frac{ab}{4\pi^2} \int_{-\pi/b}^{\pi/b} \int_{-\pi/a}^{\pi/a} \frac{e^{i\mathbf{r}_{n,m} \cdot \boldsymbol{\alpha}}}{\tilde{G}(\boldsymbol{\alpha}; a, b)} d\boldsymbol{\alpha}. \quad (54)$$

334 Within a stop band $a_{n,m}^{(f)}$ may be computed directly from (54) and the so-
 335 lution decays to zero away from the origin. Outside the stop bands, \tilde{G}
 336 vanishes along curves of constant frequency and now the double integral
 337 in (54) contains at least one line singularity in the domain of integration.
 338 Imposing an appropriate radiation condition, namely that there can be no
 339 wave energy incoming from infinity specifies how the integrals in the inverse
 340 Fourier transform (51) should be defined to interpret the effect of this line
 341 singularity. Indeed, the far field wave behaviour is entirely determined by
 342 these line singularities and we evaluate their contribution by mapping the
 343 integral domain into a orthogonal curvilinear coordinate system which is
 344 aligned to each of the curves. The line singularities can then be processed
 345 as a continuous integral along each such line. Each integral in the vari-
 346 able perpendicular to the line of singularities can be deformed appropriately
 347 around the point where it crosses the singular line—which we assume is now
 348 a simple pole—according to its effect on wave radiation at infinity.

349 Assume then that there are N_c such curves, labelled C_j , $j = 1, \dots, N_c$,
 350 along which $\tilde{G} = 0$ in the (α, β) -plane for a given fixed frequency a . We
 351 parametrise each curve by its arclength s , so that $\boldsymbol{\alpha} = \boldsymbol{\alpha}(s)$ with $|\boldsymbol{\alpha}'(s)| = 1$
 352 where the prime denotes differentiation with respect to s . Using the proce-
 353 dure outlined above it follows that, for large $|\mathbf{r}_{n,m}|$,

$$a_{n,m}^{(f)} \sim \frac{iab}{2\pi} \sum_{j=1}^{N_c} \int_{C_j} \frac{e^{i\mathbf{r}_{n,m} \cdot \boldsymbol{\alpha}(s)}}{\mathbf{n}(s) \cdot \nabla \tilde{G}} ds, \quad (55)$$

354 where $\mathbf{n}(s) = (\beta'(s), -\alpha'(s))$ denotes the unit normal to the curve C_j . For
 355 later convenience, we also define a vector $\hat{\mathbf{n}}(s) = \mu(s)\mathbf{n}(s)$, where $\mu(s) =$
 356 ± 1 , so that $\hat{\mathbf{n}}$ always points outwards from the origin. In the above, we
 357 evaluate the integrals with respect to the coordinate parallel to $\mathbf{n}(s)$ first.
 358 If $\hat{\mathbf{n}} \cdot \nabla \tilde{G} > 0$, the pole represents energy propagating away from the origin,

359 so we deform the contour and complete it in such a way that it encloses the
 360 singularity. However, if $\hat{\mathbf{n}} \cdot \nabla \tilde{G} < 0$, then energy is travelling towards the
 361 forced pin, and we deform and complete the integration contour without
 362 enclosing the pole. (In this work we have assumed that we are not at a
 363 saddle point of the dispersion surface, where $\hat{\mathbf{n}} \cdot \nabla \tilde{G} = 0$; in such a case the
 364 residue would be more complicated than those in equation 55.)

365 The next step in determining the dominant contribution as $|\mathbf{r}_{n,m}| \rightarrow \infty$
 366 is to identify stationary phase points in the oscillatory integral. These occur
 367 at P_j points on the curve C_j given by $s = s_{jk}$ when

$$\mathbf{r}_{n,m} \cdot \boldsymbol{\alpha}'(s_{jk}) = 0, \quad k = 1, \dots, P_j. \quad (56)$$

368 That is, stationary points are those points on the curve $\tilde{G} = 0$ where the
 369 radial vector to the point $\mathbf{r}_{n,m}$ is perpendicular to that curve, implying
 370 $\mathbf{r}_{n,m} = |\mathbf{r}_{n,m}| \hat{\mathbf{n}}(s)$. Applying the standard result for the method of stationary
 371 phase gives

$$a_{n,m}^{(f)} \sim \frac{iab}{\sqrt{2\pi}} \sum_{j=1}^{N_c} \sum_{k=1}^{P_j} \frac{e^{i\mathbf{r}_{n,m} \cdot \boldsymbol{\alpha}(s)} e^{i \operatorname{sgn}(\gamma(s))\pi/4}}{|\gamma(s)|^{1/2} \mathbf{n}(s) \cdot \nabla \tilde{G}} \Big|_{s=s_{jk}} \quad (57)$$

372 where $\gamma(s) = \mathbf{r}_{n,m} \cdot \boldsymbol{\alpha}''(s) = |\mathbf{r}_{n,m}| \kappa(s)$, and $\kappa(s) = \mu(s)(\beta'(s)\alpha''(s) -$
 373 $\alpha'(s)\beta''(s))$ is the curvature. Hence we may write (57) as

$$a_{n,m}^{(f)} \sim \frac{iab}{\sqrt{2\pi} |\mathbf{r}_{n,m}|} \sum_{j=1}^{N_c} \sum_{k=1}^{P_j} \frac{e^{i\mathbf{r}_{n,m} \cdot \boldsymbol{\alpha}(s)} e^{i \operatorname{sgn}(\kappa(s))\pi/4}}{|\kappa(s)|^{1/2} \mathbf{n}(s) \cdot \nabla \tilde{G}} \Big|_{s=s_{jk}}. \quad (58)$$

374 Note that if there are no stationary points then the summation above equates
 375 to zero since we are not attempting to characterise any behaviour in the far-
 376 field which decays more rapidly than $|\mathbf{r}_{n,m}|^{-1/2}$. Consequently, we have not
 377 reconstructed the wave field at infinity, but merely provided an argument
 378 for directions of wave radiation and the asymptotic form for the coefficients

379 $a_{n,m}^{(f)}$ at infinity in directions where wave radiation is permitted. Specifically,
 380 radiation is possible in those directions that cross a dispersion curve parallel
 381 to the group velocity vector at the crossing point, and where the group
 382 velocity vector also points away from the forced pin.

383 3.2. Homogeneous defect problem

384 We now consider the possibility of finding trapped modes, or localized
 385 wave motions, due to multiple defects in a doubly-periodic lattice of pinned
 386 points. A general solution is written as

$$u^{(d)}(x, y) = \sum_{n=-\infty}^{\infty} \sum_{m=-\infty}^{\infty} a_{n,m}^{(d)} g(x - na, y - mb), \quad (59)$$

387 and we set $a_{n,m}^{(d)} = 0$ for $(n, m) \in \mathcal{M}$ which represents that there is no contri-
 388 bution to the displacement from the set \mathcal{M} of pins that have been removed
 389 from the lattice. This is a homogeneous problem with no forcing, and we
 390 seek non-trivial coefficients $a_{n,m}^{(d)}$ for $(n, m) \notin \mathcal{M}$ satisfying the pin condi-
 391 tions $u^{(d)}(pa, qb) = 0$ for $(p, q) \notin \mathcal{M}$. Letting $u_{p,q}^{(d)} = u^{(d)}(pa, qb)$ represent
 392 the unknown plate displacements for $(p, q) \in \mathcal{M}$ and writing

$$u^{(d)}(x, y) = \sum_{(p,q) \in \mathcal{M}} u_{p,q}^{(d)} u^{(f)}(x - pa, y - qb), \quad (60)$$

393 we can see that $u^{(d)}(pa, qb) = 0$ if $(p, q) \notin \mathcal{M}$. To satisfy the condition that
 394 $a_{n,m}^{(d)} = 0$ if $(n, m) \in \mathcal{M}$, we note that (60) implies that

$$a_{n,m}^{(d)} = \sum_{(p,q) \in \mathcal{M}} u_{p,q}^{(d)} a_{n-p, m-q}^{(f)}, \quad (61)$$

395 so if $(n, m) \in \mathcal{M}$

$$0 = \sum_{(p,q) \in \mathcal{M}} u_{p,q}^{(d)} a_{n-p, m-q}^{(f)}, \quad \text{for } (n, m) \in \mathcal{M}. \quad (62)$$

396 Thus, we have a homogeneous system for the unknown displacements $u_{p,q}^{(d)}$
 397 at the defects. In other words, the determinant of the matrix

$$K_{n,m,p,q} = a_{n-p,m-q}^{(f)}, \quad (n, m), (p, q) \in \mathcal{M}, \quad (63)$$

398 is required to vanish for trapping solutions to exist (since we require that
 399 $u_{p,q}^{(d)}$, $(p, q) \in \mathcal{M}$ are not all zero). The Toeplitz matrix K is sized $N \times N$,
 400 where N represents the number of defect points contained in the set \mathcal{M} .
 401 Computing the kernel of K allows us to calculate the corresponding trapped
 402 mode(s) from (60). In practice this can be done by finding the eigenvector(s)
 403 of K with eigenvalue zero. If the $u_{p,q}^{(d)}$ were all zero, then the lattice may
 404 as well have been pinned periodically with no defects, and we return to the
 405 Bloch-Floquet problem discussed earlier where trapping solutions cannot
 406 exist.

407 To compute the shape of the trapped modes inside the defect we need
 408 to compute the nonzero $u_{p,q}^{(d)}$ given in (62). This is done by first determining
 409 the kernel of the Toeplitz matrix K from which we can then compute the
 410 scattering coefficients in (61) allowing us to construct the displacement (59)
 411 after suitable truncation of both sums.

412 Since G is real, if we work at frequencies a that lie in a stop band (so that
 413 G does not vanish in the domain integral in (51)) then we are assured that
 414 $a_{n,m}^{(f)}$ is real and hence the determinant of $K_{n,m,p,q}$ is also real. Thus, the task
 415 of finding trapping solutions is simply one of finding real frequencies that
 416 force a real determinant to vanish. We note that the realness and symmetry
 417 of $K_{n,m,p,q}$ implies that the number of linearly independent trapped modes
 418 is equal to the multiplicity of the zero eigenvalue.

419 It is instructive to consider the case where there is only a single defect
 420 at the origin, so that $\mathcal{M} = \{(0, 0)\}$ and then from (61) the requirement for

421 a trapped mode (51) is simply

$$0 = a_{0,0}^{(f)} = \frac{1}{4\pi^2} \int_0^\pi \int_0^\pi \frac{1}{G(\theta, \phi; a, b)} d\theta d\phi. \quad (64)$$

422 Clearly, for solutions of (64) to exist, we require G^{-1} to take different
 423 signs in the domain $0 < \theta, \phi < \pi$. Since $\lambda(t_0) = -i(1 - \theta^2)^{1/2}$ where $t_0 \in$
 424 $(0, 1)$ we see immediately that $G^{-1}(\theta, \phi; a, b) = 0$ along the circle $\theta^2 + \phi^2 = 1$.
 425 This provides a good motivation for seeking a trapped mode solution. For
 426 larger values of a , where $|t_n| < 1$ for values of n other than zero, G^{-1}
 427 also vanishes along curves $\phi^2 + (\theta + 2n\pi/a)^2 = 1$, but such arguments are
 428 redundant as numerical results would suggest that such values of a lie outside
 429 a stop band.

430 3.3. Lines of defects: Fabry-Perot resonances

431 Assume now that entire rows are left unpinned in the otherwise doubly-
 432 periodic array of pinned points. For such a configuration we seek solutions
 433 which are trapped by the lines of defects and rapidly decay away from the
 434 defect line. Such solutions are often referred to as Fabry-Perot resonances,
 435 or waveguide modes. The missing pins are assumed to lie along the rows
 436 $y = mb$ where $m \in \mathcal{M} \subset \mathbb{Z}$. In the simplest case where a single line of
 437 pins are removed along $y = 0$, $\mathcal{M} = \{0\}$. The general solution can be
 438 written as in (59) with $a_{n,m}^{(d)} = 0$ for $n \in \mathbb{Z}$ and $m \in \mathcal{M}$. Clearly there is
 439 no periodicity in the array in the y direction, but the array is now periodic
 440 in the x -direction. Consequently any solution must be quasi-periodic in x ;
 441 that is, they must satisfy

$$u^{(d)}(x + pa, y) = u^{(d)}(x, y)e^{ip\theta}, \quad (65)$$

442 where, unlike in previous sections, θ is a freely-chosen parameter which
 443 reflects the quasi-periodicity of the solution whilst $p \in \mathbb{Z}$. Consequently

444 (this can be shown by using (65) in (59)), $a_{n,m}^{(d)} = a_{0,m}^{(d)} e^{in\theta}$ and (59) becomes

$$u^{(d)}(x, y) = \sum_{m=-\infty}^{\infty} a_{0,m}^{(d)} \sum_{n=-\infty}^{\infty} e^{in\theta} g(x - na, y - mb). \quad (66)$$

445 We then apply the pinned conditions $u_{0,q}^{(d)} \equiv u^{(d)}(0, qb) = 0$ for $q \notin \mathcal{M}$,
 446 which only has to be made along $x = 0$, since all other values of x have been
 447 accounted for by (65). This gives

$$\sum_{m=-\infty}^{\infty} a_{0,m}^{(d)} \sum_{n=-\infty}^{\infty} e^{-in\theta} g(na, (q - m)b) = \sum_{q \in \mathcal{M}} u_{0,q}^{(d)} \delta_q \quad (67)$$

448 where $u_{0,q}^{(d)}$ are the unknown plate displacements along $(x, y) = (0, qb)$; that
 449 is, along the cross-section $x = 0$ perpendicular to the line of defects. Multi-
 450 plying (67) by $e^{-iq\phi}$ and summing over all q transforms (67) into

$$A^{(d)}(\phi) G(\theta, \phi; a, b) = \sum_{q \in \mathcal{M}} u_{0,q}^{(d)} e^{-iq\phi}, \quad (68)$$

451 where we now have

$$A^{(d)}(\phi) = \sum_{m=-\infty}^{\infty} a_{0,m}^{(d)} e^{-im\phi}, \quad (69)$$

452 and G is the double-lattice sum for the infinite periodic array defined as in
 453 (45). The θ -dependence is implicit in $A^{(d)}$ and $u_{0,q}^{(d)}$.

454 Rearranging (68) for $A^{(d)}(\phi)$, inverting the transform defined in (69) to
 455 return to $a_{0,m}^{(d)}$, and then applying the conditions $a_{0,m}^{(d)} = 0$ for $m \in \mathcal{M}$ gives
 456 the homogeneous system of equations

$$0 = \sum_{q \in \mathcal{M}} u_{0,q}^{(d)} \int_{-\pi}^{\pi} \frac{e^{i(m-q)\phi}}{G(\theta, \phi; a, b)} d\phi, \quad m \in \mathcal{M}. \quad (70)$$

457 Thus, for a Fabry-Perot resonance or trapped mode, we require the deter-
 458 minant of the Toeplitz matrix

$$K_{m,q}^{(d)} = \int_0^{\pi} \frac{\cos((m-q)\phi)}{G(\theta, \phi; a, b)} d\phi, \quad m, q \in \mathcal{M}, \quad (71)$$

459 to vanish. We note again that G is real, so provided it is also non-zero for
460 $0 < \phi < \pi$ for a given value of θ , the integral (71) is real and the determinant
461 of the matrix defined by (71) is also real.

462 **4. Results and discussion**

463 *4.1. Forcing and scattering in one dimensional arrays*

464 We begin by considering the one dimensional array problem of a forced
465 pin (a defect subject to time harmonic forcing of unit amplitude), which
466 is shown for an array of period $a = 2\pi$ in Figure 1(a). In this figure we
467 can see clear left-right and up-down symmetry in the computed field, as
468 well as clear energy radiation as we move away from the forcing location
469 at the origin. As outlined in section 2.2, we show that it is possible to
470 express the unknown coefficients for the scattering problem in terms of the
471 coefficients for the forcing problem. This leads us to Figure 1(b), where the
472 total field is computed for a particular scattering problem. A plane wave
473 is normally-incident on the array from $y > 0$, so that $\theta_0 = 0$ with $a = \pi$.
474 In this configuration no other diffraction orders are excited, and so we can
475 determine the reflection and transmission coefficients straightforwardly as
476 $R = |R_0|^2 = 0.67801$ and $T = |T_0|^2 = 0.32199$.

477 Thus the symmetry of the plate displacement about the line of pins
478 shown in Figure 1(b) is due to it being a particular snapshot in time of the
479 superposition of a totally transmitted plane wave and a symmetric circular
480 outgoing wave from the defect. Vertical channels of minimal displacement
481 can be observed both above and below this single defect. We also observe a
482 focusing of energy at the origin where the pin has been removed. Referring
483 to Figure 3(a) of Evans and Porter [7], when $\theta_0 = 0$ the cut-off frequency

484 between the zeroth and higher grating orders is at $a = ka' = 2\pi$ where the
485 reflected wave energy is precisely zero.

486 For a plane wave with incident angle $\theta_0 = \pi/6$ Figure 2(a) shows a
487 snapshot in time of a different scattered wave pattern. In this plot we can
488 clearly see the formation of partial standing waves above the grating, caused
489 by a large amount of reflection of wave energy by the array (as previously,
490 no other diffraction orders are excited and so $R = |R_0|^2 = 0.87550$ and
491 $T = |T_0|^2 = 0.12449$). However below the grating we can see the interaction
492 effect between the transmitted wave energy and circular waves emanating
493 from the defect, with occasional destructive interference being produced to
494 the left of the defect.

495 Using our formulation we can also consider the effects of multiple pins
496 being removed, as shown in Figure 2(b) where for a single array of period $a =$
497 2 , four defects have been removed to recreate a double-slit experiment. For
498 this problem we consider an incident wave at $\theta_0 = \pi/12$, which corresponds
499 to a higher level of energy transmission ($R = |R_0|^2 = 0.57652$ and $T =$
500 $|T_0|^2 = 0.42348$). Here the circular waves emanating from the defects also
501 have a strong effect, with a clear channel of minimal displacement directed
502 downwards and to the right from the right hand defect.

503 *4.2. Forcing and band surfaces for doubly periodic arrays*

504 We now consider the problem of determining the band surfaces of our
505 pinned plate, which allows us to determine information about the propa-
506 gating modes, or Bloch modes, that are supported by our doubly periodic
507 medium [29]. From this, the band surfaces also reveal the locations of *full* or
508 *partial stop bands*, which correspond to frequencies at which no propagation
509 through the array is possible, for given (θ, ϕ) values. It is in these stop bands

510 that we look for trapping behaviour when defects are introduced.

511 Movchan et al. [10] considered the particular case of a square array of
512 pins ($b/a = 1$) by taking limits of a more general system based on multi-
513 pole expansions designed to investigate the band-gap structure of periodic
514 arrays of finite-radius circular holes. Thus, when the radius of a clamped
515 hole tended to zero, a simplified dispersion relation was derived in terms
516 of lattice sums for the Helmholtz and modified Helmholtz equations [see
517 equation 6.2 in 10]. As outlined in their paper the computation of these
518 lattice sums is extremely complicated [also see 28]. Here, we have derived
519 an alternative dispersion relation (52) in which the lattice sum (49) is both
520 convergent and simple to compute. Our solutions coincide with those of [10]
521 who were also able to determine that the band surfaces for arrays of pins
522 were bound between singularities arising from these lattice sums. These sin-
523 gularity curves correspond to discrete values at which plane wave solutions
524 would be supported in the medium in the absence of our pins [30]. This
525 acts as a useful tool for computing solutions of (52) as an upper and lower
526 bound for each zero can be determined straightforwardly.

527 To determine the band surfaces from (52) we search for values of a (which
528 is a dimensionless proxy for the wavenumber) for given values of θ and ϕ
529 (which are themselves proxies for Bloch vector elements). For the case of
530 a square array ($b/a = 1$) we show the first, second and third band surfaces
531 in Figures 3(a), 3(b) and 3(c) (respectively) over a quarter of the Brillouin
532 zone. A full picture of the band surface over the entire Brillouin zone can be
533 obtained by reflection in the θ and ϕ axes. From the picture of the first band
534 surface we can deduce that we have a complete stop band from $0 < a < \pi$,
535 and by comparing Figures 3(a) and 3(b), that only partial stop bands exist
536 between the first and second band surfaces (i.e. the stop band frequency

537 depends on θ and ϕ). Movchan et al. [10] show that only partial stop bands
538 exist between all other higher order band surfaces. Additionally, we note
539 that the width of the first stop band is proportional to the spacing ratio
540 b/a , that is, the first stop band exists in the range $0 < a < \pi/(b/a)$ for
541 rectangular arrays, as outlined in section 3.1.

542 In section 3.1 it was shown that wave radiation through the array from
543 a forced pin can only occur when the Bloch vector α and the vector tangent
544 to a constant frequency curve on the dispersion surface are at right angles,
545 and provided the gradient of the dispersion surface also points away from
546 the origin at any such points. Then the amplitude of the wave radiated to
547 infinity is inversely proportional to both the magnitude of that gradient and
548 to the square root of the curvature of the curve of constant frequency.

549 Now, since $b/a = 1$, directions in α -space are the same as in (θ, ϕ) -space.
550 Moreover, if wave propagation is possible in a certain direction in α -space,
551 then it is also possible in the same direction in (x, y) -space. Thus, observing
552 Figures 3(a) and 3(b) we can say the following. For $0 < a < \pi$ there is no
553 wave radiation to infinity as the frequency lies in a stop band. Then, as a
554 increases from π to approximately 3.6238 (the level of the saddle point) there
555 is still no wave radiation as the only possible directions for wave propagation
556 are along $x = 0$ and $y = 0$, but there the gradient of the dispersion surface
557 along outgoing lines is negative. As a increases beyond 3.6238, again the
558 lines $x = 0$ and $y = 0$ are excluded from wave radiation as the gradient is
559 negative but wave radiation along $x = y$ (and by reflection along $x = -y$)
560 is allowed, determined by values of θ and ϕ in the portion of the dispersion
561 surface for which the gradient is positive. The amplitude factor of radiated
562 waves is large for a close to the value at the saddle point where the gradient
563 is close to zero (this makes sense, as the group velocity is small and so

564 energy propagates slowly away from the origin) and decreases as a increases
565 up to the the point at which we switch from the first band to the second
566 band ($a \simeq 4.4429$). According to the second band, all possible directions
567 of wave radiation are associated with negative gradients on the dispersion
568 surface and therefore there is no wave radiation to infinity associated with
569 this band. However, moving on to Figure 3(c), we can see that the third
570 band also starts at $a \simeq 4.4429$ and in this case there are possible directions
571 of wave radiation to infinity along $x = 0$ and $y = 0$ for values between
572 $a \simeq 6.3137$ and $a \simeq 7.0248$ where the gradients of the dispersion surfaces
573 are increasing.

574 The overall picture is one in which the scope to radiate waves from an
575 oscillating source at the origin to infinity is limited, even if the frequency
576 is inside a band surface. However, we have shown that oscillations within
577 certain higher frequency ranges can send waves through the lattice in differ-
578 ent directions (here either along $x = y$ for $3.6238 < a < 4.4429$ or along the
579 axes if $6.3137 < a < 7.0248$).

580 In Figure 4 we show a snapshot in time of the plate displacement when
581 a central pin in a doubly-periodic pinned plate is made to oscillate with
582 unit amplitude at a dimensionless value of $a = 1$ and spacing ratio of $b/a =$
583 $1/2$. This corresponds to a frequency within the stop band for the doubly-
584 periodic array ($0 < a < 2\pi$ when $b/a = 1/2$) and hence the figure confirms
585 that there is no energy propagation to infinity. Indeed, the displacement is
586 predominantly contained horizontally within one layer of pins, and contained
587 vertically within two layers.

588 *4.3. Trapped modes in doubly periodic arrays with defects*

589 We now examine the different mode shapes that can be supported inside
590 defects which exist in doubly periodic square arrays. We look for the reso-
591 nant frequencies of these defects inside the first stop band, which for square
592 arrays ($b/a = 1$) is the interval $0 < a < \pi$. Each trapped mode correspond-
593 ing to a non-degenerate frequency was also confirmed by exciting a large
594 finite cluster, with the same defect in its centre, with an incident wave. At
595 degenerate frequencies, different combinations of the two possible trapped
596 modes appeared, depending on the angle of incidence and the relative close-
597 ness of the frequencies. It would be an interesting problem to attempt to
598 predict how the excited modes depend on this angle, but one which is not
599 attempted here.

600 We begin by determining the resonant frequencies for two problems –
601 firstly, a single defect at the origin, and secondly, a 3×3 sized defect cluster
602 centred about the origin where pins corresponding to the indices $(-1, 0, 1) \times$
603 $(-1, 0, 1)$ are removed. This is done by evaluating the determinant of the
604 Toeplitz matrix $K_{m,n,p,q}$ as given in (63) for varying a . We can see from
605 Figure 5(a) that only one resonant frequency exists in the first stop band
606 for the single defect problem and is given by $a \simeq 2.53727$. This compares
607 well with the estimate $a \simeq 2.538$ given in McPhedran et al. [31] which was
608 evaluated by computing the kernel of a truncated matrix of standard Green’s
609 functions (of the form given in (7)).

610 For the 3×3 defect we can see from Figure 5(b) that there are res-
611 onant frequencies at $a \simeq 1.35692$, 1.95271 , 2.38206 , 2.61818 , 2.62461 and
612 $a \simeq 2.93110$. In this case we have the added complication of degenerate
613 (repeated) roots corresponding to the determinant curve touching the zero
614 axis as opposed to crossing it completely. These degenerate frequencies are

615 a consequence of the symmetry of the geometry and the associated trapped
616 mode. That is, it is possible for two modes to exist for the same frequency a ,
617 one with a line of symmetry in $x = 0$ and the other in $y = 0$. If $a/b \neq 1$ then
618 modes symmetric in x are different to modes symmetric in y , eliminating
619 the presence of repeated roots.

620 The discontinuity of the determinant curve in Figure 5(b) at $a = 2.82743$
621 is associated with the determinant of K becoming infinitely large. This is
622 a consequence of the Green's function being undefined at this value of a for
623 all $0 < \theta < \pi$ (when $b/a = 1$), and does not correspond to a trapped mode.

624 Returning to the single defect problem, the mode shape corresponding
625 to $a \simeq 2.53728$ is computed in Figure 6 which shows one peak, symmetric
626 about both $x = 0$ and $y = 0$ which is well trapped inside the defect with
627 negligible displacement throughout the surrounding array.

628 For the 3×3 defect the associated modes are given in Figure 7. A number
629 of these mode shapes have clear reflection and rotational symmetry inside
630 the defect, most notably those corresponding to the degenerate frequencies
631 which are given in Figures 7(b), 7(e), and 7(f). Some of the mode shapes
632 computed here are reminiscent of the mode shapes for square plates that are
633 completely clamped, as discussed in [32]. Again, we observe a rapid decay of
634 displacement with distance away from the defect into the array in all figures.

635 We finally consider a 4×1 defect in a square array ($b/a = 1$), for which
636 all trapped mode frequencies are distinct (i.e. not repeated roots) in the
637 first stop band. The corresponding mode shapes are given in Figure 8 and
638 bear resemblance to the first few harmonics for waves on a string, which is
639 not unexpected given the slender geometry of our defect cluster.

640 *4.4. Fabry-Perot line defects in two dimensional arrays*

641 For the waveguide problem, we remove entire rows of pins from the
642 otherwise perfect doubly periodic array. We then vary our quasi-periodicity
643 parameter θ and look for values of a that satisfy the relation given by (71),
644 which essentially reveals the frequencies at which different waveguide modes
645 are supported inside the defect(s). These waveguide modes transport wave
646 energy inside the line defects with minimal (and strongly decaying) leakage
647 into the surrounding array.

648 In Figure 9(a) we examine (71) for the case of a single line defect ($m = 0$)
649 for multiple aspect ratios b/a . We can see that for this single line defect
650 ($b/a = 1$) we have a single curve which exists in the interval $1.96720 < a < \pi$.
651 We see similarly sloped curves for $b/a = 1.5$ and $b/a = 2$, which end abruptly
652 when they approach the edge of their first stop bands (for the instance when
653 $b/a = 2$, the stop band interval is $0 < a < \pi/2$).

654 In Figure 9(b) we consider the case when we have two non-neighbouring
655 line defects ($m = 0, -3$) for multiple aspect ratios b/a . For $b/a = 1$, (71)
656 reveals two unique values of a over an interval of θ values, which corresponds
657 to one symmetric mode and one antisymmetric mode supported across both
658 line defects (represented by the broken and solid lines respectively). In a
659 small interval near $\theta \simeq 2.25$ the waveguide mode frequencies a become nearly
660 degenerate but ultimately two modes exist. The curves for $b/a = 1.5$ and
661 $b/a = 2$ are quite different however, as we see increasing degeneracy with
662 increasing θ , and no clear splitting near the approach to the first stop band
663 when compared to the $b/a = 1$ curve.

664 For the single line defect problem, the waveguide mode corresponding to
665 $b/a = 1$, $a = 2.1$, $\theta = 0.87850$ is computed using (66) and shown in Figure
666 10(a). This mode is well contained with small, rapidly decaying peaks exist-

667 ing outside the defect when the mode itself is at a minimum. For the doubly
668 periodic problem, the waveguide mode corresponding to $b/a = 1$, $a = 2 \cdot 1$,
669 $\theta = 0.75567$ is given in Figure 10(b) and in Figure 10(c) the mode corre-
670 sponding to $\theta = 0.97115$ is shown. From Figure 10(b) we can take a vertical
671 slice through the field and determine that this first mode is antisymmetric,
672 and as before, we have some leakage outside the array corresponding to the
673 minimum peaks of the mode, with little interaction in the space between the
674 two channels. For Figure 10(c) we have the second waveguide mode which
675 is symmetric and demonstrates minimal leakage outside the line defects for
676 $x < 0$, however, there is a now strong interaction between the two channel
677 defects.

678 5. Conclusions

679 In this paper we have examined a number of problems connected with
680 defects in one- and two-dimensional rectangular arrays of periodically pinned
681 plates. A method has been outlined for analytically determining a variety
682 of properties of the solution including the plate displacement for problems
683 where a single pin within the array is forced to oscillate and where incident
684 waves are diffracted by a one-dimensional pinned array in which multiple
685 pins are removed. For two-dimensional arrays, we have also provided an-
686 alytical expressions to determine certain localized modes which exist when
687 either a finite number of pins are removed or entire rows are removed. Con-
688 nections between forced pin problems and scattering and trapping problems
689 in which pins are removed have been highlighted in both one- and two-
690 dimensional problems. This has similarities to the work of Thompson and
691 Linton [15] for a related problem in acoustics. The exact description of the

692 infinite array has been included by Fourier transforming infinite systems of
693 equations, thus avoiding the use of supercell methods as in Poulton et al.
694 [22] or by interpreting results from a truncated array approximation.

695 We have shown theoretically how to determine directions and amplitude
696 factors of wave radiation through a doubly-periodic array in which the cen-
697 tral pin is forced to oscillate and shown that different frequency ranges lead
698 to wave radiation in different directions.

699 There are a number of interesting extensions to the current work that
700 could be made. For example, the problem of plane wave scattering by either
701 one- or two-dimensional semi-infinite periodic arrays of pins could be solved
702 using the discrete Wiener-Hopf technique as done by [33] and [34] for scat-
703 tering of long waves by cylinders. Defects (particularly line defects) could
704 also be put introduced into their formulations in a relatively straightforward
705 manner.

706 Another straightforward extension of the methods presented here can be
707 made for problems involving defects in a semi-infinite elastic plate which is
708 pinned periodically along its free edge. The solution for the corresponding
709 problem without defects has been presented in [35] which simply requires
710 that the Green's function, representing the effect of each pin be altered, to
711 take account of the free edge conditions [see 36].

712 In the final stages of preparation of this paper, the authors became aware
713 of related work published by [37], which independently reproduces some of
714 the results here. Specifically they consider the problems of single point
715 and line defects (as opposed to the interaction theory developed herein to
716 accommodate multiple defects). They also considered forcing and defects in
717 doubly periodic arrays of point masses, as well as rigid pins.

718 **References**

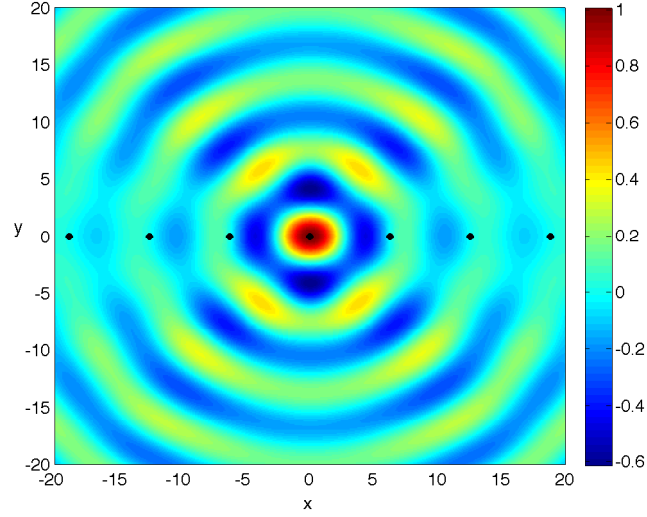
- 719 [1] F. Leppington, Acoustic scattering by membranes and plates with line
720 constraints, *Journal of Sound and Vibration* 58 (3) (1978) 319–332.
- 721 [2] D. Crighton, Transmission of energy down periodically ribbed elastic
722 structures under fluid loading, *Proceedings of the Royal Society of Lon-*
723 *don. A. Mathematical and Physical Sciences* 394 (1807) (1984) 405–436.
- 724 [3] M. Spivack, Wave propagation in finite periodically ribbed structures
725 with fluid loading, *Proceedings of the Royal Society of London. Series*
726 *A: Mathematical and Physical Sciences* 435 (1895) (1991) 615–634.
- 727 [4] M. Sobnack, D. Crighton, Effect of an isolated irregularity on the trans-
728 mission of energy down a periodically ribbed fluid-loaded elastic struc-
729 ture, *Proceedings of the Royal Society of London. Series A: Mathemat-*
730 *ical and Physical Sciences* 441 (1913) (1993) 473–494.
- 731 [5] A. Cooper, D. Crighton, Transmission of energy down periodically
732 ribbed elastic structures under fluid loading: spatialperiodicity in the
733 pass bands, *Proceedings of the Royal Society of London. Series A: Math-*
734 *ematical, Physical and Engineering Sciences* 454 (1979) (1998) 2893.
- 735 [6] M. Sobnack, D. Crighton, Anderson localization effects in the trans-
736 mission of energy down an irregularly ribbed fluid-loaded structure,
737 *Proceedings of the Royal Society of London. Series A: Mathematical*
738 *and Physical Sciences* 444 (1920) (1994) 185–200.
- 739 [7] D. Evans, R. Porter, Penetration of flexural waves through a period-
740 ically constrained thin elastic plate in vacuo and floating on water,
741 *Journal of Engineering Mathematics* 58 (1) (2007) 317–337.

- 742 [8] D. Evans, R. Porter, Wave diffraction by a periodically constrained
743 elastic plate floating on water, in: Proceedings of the 21st International
744 Workshop on Water Waves and Floating Bodies, Loughborough, UK,
745 2006.
- 746 [9] P. Martin, Multiple scattering: interaction of time-harmonic waves with
747 N obstacles, vol. 107, Cambridge Univ Pr, 2006.
- 748 [10] A. Movchan, N. Movchan, R. McPhedran, Bloch–Floquet bending
749 waves in perforated thin plates, Proceedings of the Royal Society A:
750 Mathematical, Physical and Engineering Science 463 (2086) (2007)
751 2505–2518.
- 752 [11] N. Movchan, R. McPhedran, A. Movchan, C. Poulton, Wave scattering
753 by platonic grating stacks, Proceedings of the Royal Society A: Mathe-
754 matical, Physical and Engineering Science 465 (2111) (2009) 3383–3400.
- 755 [12] S. Haslinger, N. Movchan, A. Movchan, R. McPhedran, Transmission,
756 trapping and filtering of waves in periodically constrained elastic plates,
757 Proceedings of the Royal Society A: Mathematical, Physical and Engi-
758 neering Science 468 (2137) (2011) 76–93.
- 759 [13] M. Meylan, R. McPhedran, Fast and slow interaction of elastic waves
760 with platonic clusters, Proceedings of the Royal Society A: Mathemat-
761 ical, Physical and Engineering Science 467 (2136) (2011) 3509–3529.
- 762 [14] W. Parnell, P. Martin, Multiple scattering of flexural waves by random
763 configurations of inclusions in thin plates, Wave Motion 48 (2) (2011)
764 161–175.

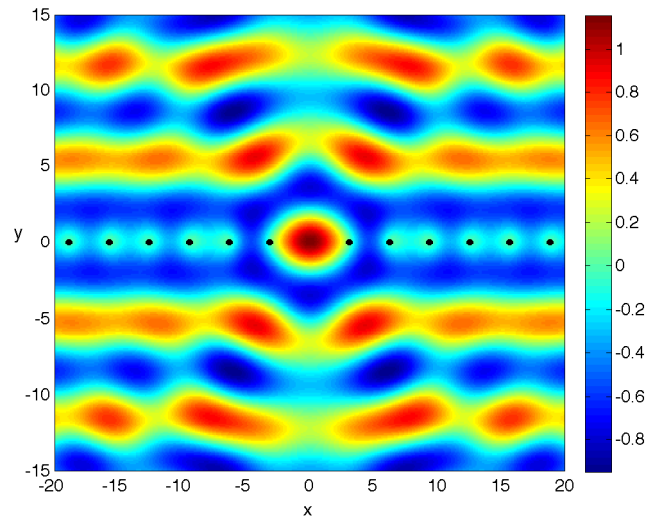
- 765 [15] I. Thompson, C. Linton, An interaction theory for scattering by defects
766 in arrays, *SIAM Journal on Applied Mathematics* 68 (6) (2008) 1783–
767 1806.
- 768 [16] I. Thompson, C. Linton, On the excitation of a closely spaced array
769 by a line source, *IMA journal of applied mathematics* 72 (4) (2007)
770 476–497.
- 771 [17] M. Sigalas, Elastic wave band gaps and defect states in two-dimensional
772 composites, *Journal of the Acoustical Society of America* 101 (3) (1997)
773 1256–1261.
- 774 [18] A. Khelif, A. Choujaa, B. Djafari-Rouhani, M. Wilm, S. Ballandras,
775 V. Laude, Trapping and guiding of acoustic waves by defect modes in
776 a full-band-gap ultrasonic crystal, *Physical Review B* 68 (21) (2003)
777 214301.
- 778 [19] S. Wilcox, L. Botten, R. McPhedran, C. Poulton, C. de Sterke, Mod-
779 eling of defect modes in photonic crystals using the fictitious source
780 superposition method, *Physical Review E* 71 (5) (2005) 056606.
- 781 [20] H. Ammari, F. Santosa, Guided waves in a photonic bandgap structure
782 with a line defect, *SIAM Journal on Applied Mathematics* (2004) 2018–
783 2033.
- 784 [21] S. Mahmoodian, R. McPhedran, C. de Sterke, K. Dossou, C. Poul-
785 ton, L. Botten, Single and coupled degenerate defect modes in two-
786 dimensional photonic crystal band gaps, *Physical Review A* 79 (1)
787 (2009) 013814.

- 788 [22] C. Poulton, R. McPhedran, N. Nicorovici, L. Botten, Localized Greens
789 functions for a two-dimensional periodic material, in: IUTAM Sympto-
790 sium on Asymptotics, Singularities and Homogenisation in Problems of
791 Mechanics, Springer, 181–190, 2004.
- 792 [23] A. Figotin, V. Goren, Resolvent method for computations of localized
793 defect modes of H-polarization in two-dimensional photonic crystals,
794 Physical Review E 64 (5) (2001) 056623.
- 795 [24] D. Kan, A. Asatryan, C. Poulton, L. Botten, Multipole method for
796 modeling linear defects in photonic woodpiles, JOSA B 27 (2) (2010)
797 246–258.
- 798 [25] C. Poulton, L. Botten, R. McPhedran, A. Movchan, Source-neutral
799 Green’s functions for periodic problems in electrostatics, and their
800 equivalents in electromagnetism, Proceedings of the Royal Society of
801 London. Series A: Mathematical, Physical and Engineering Sciences
802 455 (1983) (1999) 1107–1123.
- 803 [26] A. Movchan, N. Movchan, C. Poulton, Asymptotic models of fields in
804 dilute and densely packed composites, Imperial College Press London,
805 2002.
- 806 [27] S. Chin, N. Nicorovici, R. McPhedran, Green’s function and lattice
807 sums for electromagnetic scattering by a square array of cylinders, Phys-
808 ical Review E 49 (1994) 4590–4602.
- 809 [28] C. Linton, Lattice sums for the Helmholtz equation, SIAM review 52 (4)
810 (2010) 630–674.

- 811 [29] J. Joannopoulos, Photonic crystals: molding the flow of light, Princeton
812 University Press, 2008.
- 813 [30] S. Guo, P. McIver, Propagation of elastic waves through a lattice of
814 cylindrical cavities, Proceedings of the Royal Society A: Mathematical,
815 Physical and Engineering Science 467 (2134) (2011) 2962–2982.
- 816 [31] R. McPhedran, A. Movchan, N. Movchan, Platonic crystals: Bloch
817 bands, neutrality and defects, Mechanics of Materials 41 (4) (2009)
818 356–363.
- 819 [32] A. W. Leissa, Vibration of plates, NASA SP-160, Washington D. C.,
820 1969.
- 821 [33] C. M. Linton, P. A. Martin, Semi-infinite arrays of isotropic point scat-
822 terers. A unified approach, SIAM J. Appl. Math. 64 (2004) 1035–1056.
- 823 [34] N. Tymis, I. Thompson, Low-frequency scattering by a semi-infinite
824 lattice of cylinders, The Quarterly Journal of Mechanics and Applied
825 Mathematics 64 (2) (2011) 171–195.
- 826 [35] D. Evans, R. Porter, Flexural waves on a pinned semi-infinite thin
827 elastic plate, Wave Motion 45 (6) (2008) 745–757.
- 828 [36] R. Gunda, S. Vijayakar, R. Singh, J. Farstad, Harmonic Greens func-
829 tions of a semi-infinite plate with clamped or free edges, The Journal
830 of the Acoustical Society of America 103 (1998) 888–899.
- 831 [37] C. Poulton, A. Movchan, N. Movchan, R. McPhedran, Analytic theory
832 of defects in periodically structured elastic plates, Proceedings of the
833 Royal Society A: Mathematical, Physical and Engineering Science .

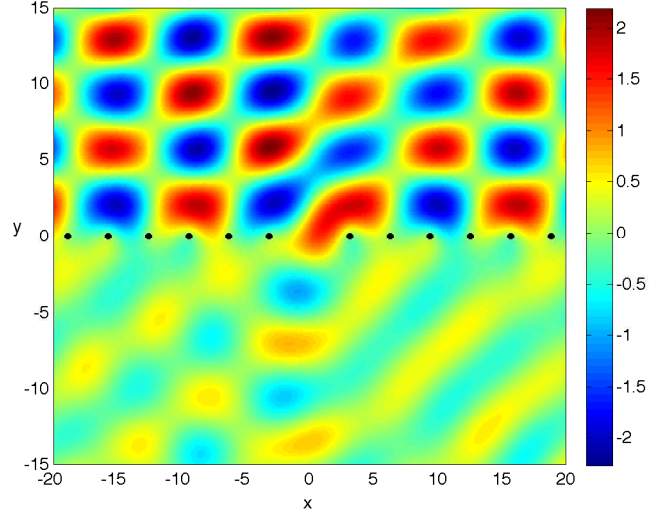


(a)

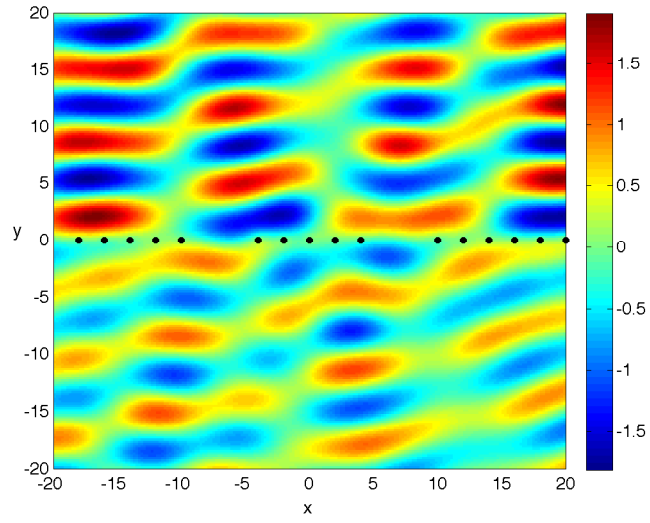


(b)

Figure 1: (a): Total field ($\text{Re}\{u^{(f)}\}$) for a single array of period $a = 2\pi$ with a single defect at $\mathcal{M} = \{0\}$ when the central pin is forced. (b): Total field ($\text{Re}\{u^{(s)}\}$) demonstrating scattering by a plane wave at normal incidence on an array with $a = \pi$, $\mathcal{M} = \{0\}$.

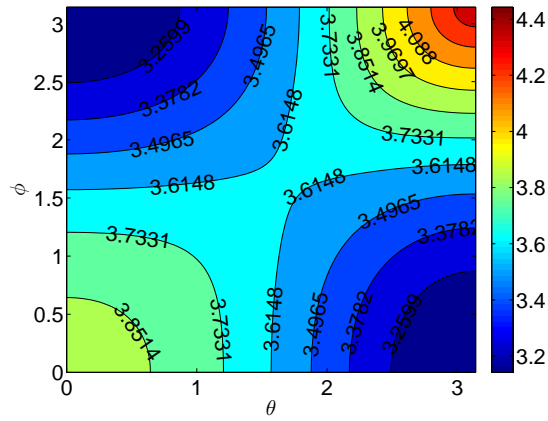


(a)

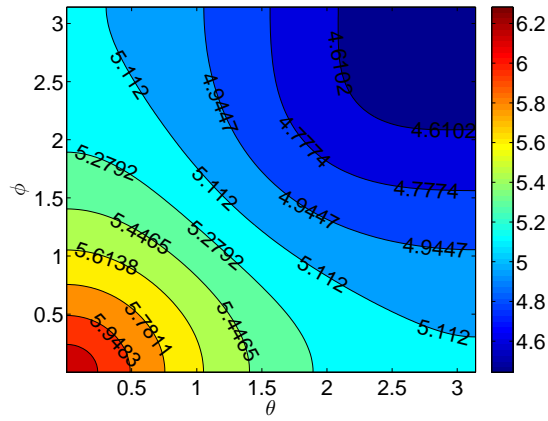


(b)

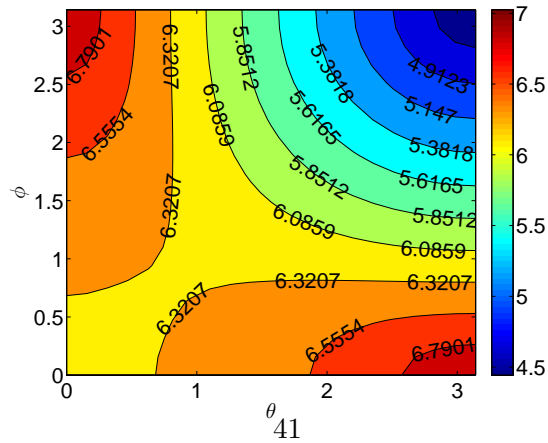
Figure 2: (a): Total field ($\text{Re}\{u^{(s)}\}$) demonstrating scattering by a plane wave at angle $\theta_i = \pi/6$ on a grating of period $a = \pi$. (b): Total field ($\text{Re}\{u^{(s)}\}$) demonstrating scattering by a plane wave at angle $\theta_i = \pi/12$ incident on a single array of period $a = 2$ with a four defects at index locations $\mathcal{M} = \{-4, -3, 3, 4\}$.



(a)



(b)



(c)

Figure 3: (a): Contour plot of a values constituting the first band surface, over $1/4$ of the Brillouin zone, for a doubly periodic square array of pinned points $b/a = 1$. Figures (b) and (c) show the second and third band surfaces (respectively) over $1/4$ of the Brillouin zone.

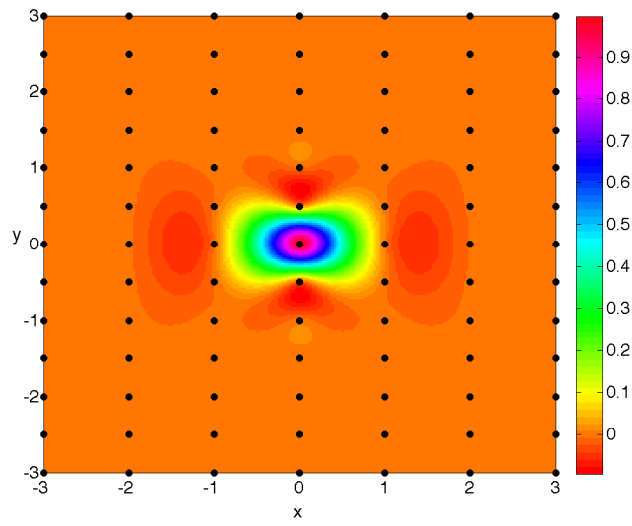
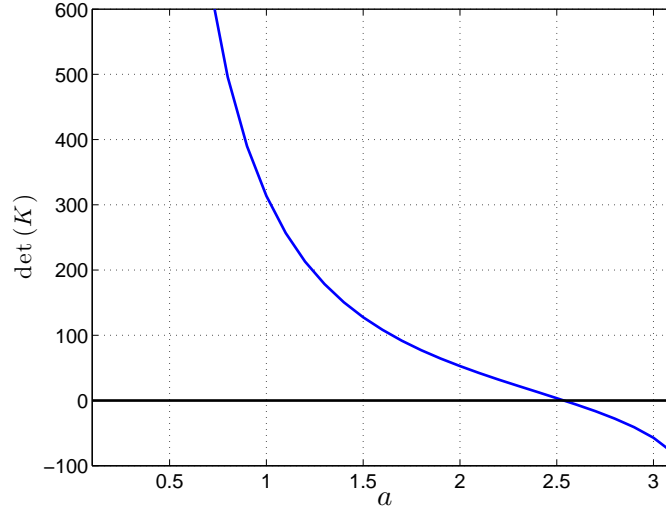
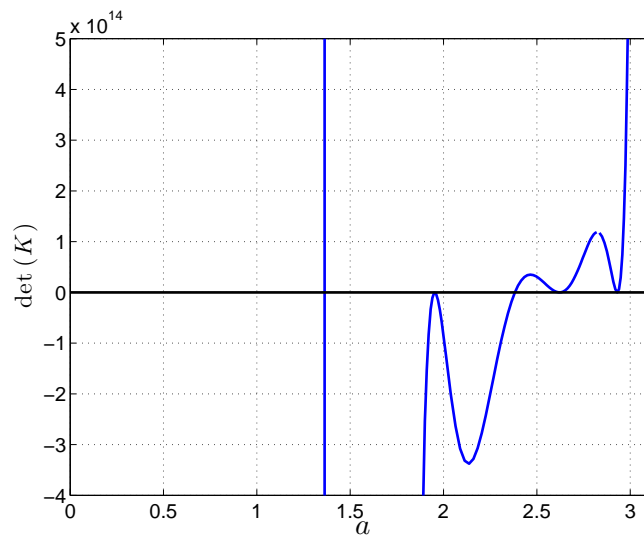


Figure 4: Total field ($\text{Re}\{u^{(f)}\}$) for the forcing of the central pin $\mathcal{M} = \{0, 0\}$ in a doubly periodic array with periodicity $a = 1$, $b = 1/2$.



(a)



(b)

Figure 5: (a): Determinant of Toeplitz matrix $K_{m,n,p,q}$ for a single defect at the origin, with a single defect frequency at $a \simeq 2.53728$ for $b/a = 1$. (b): Determinant of Toeplitz matrix $K_{m,n,p,q}$ for a 3×3 defect, with multiple defect frequencies.

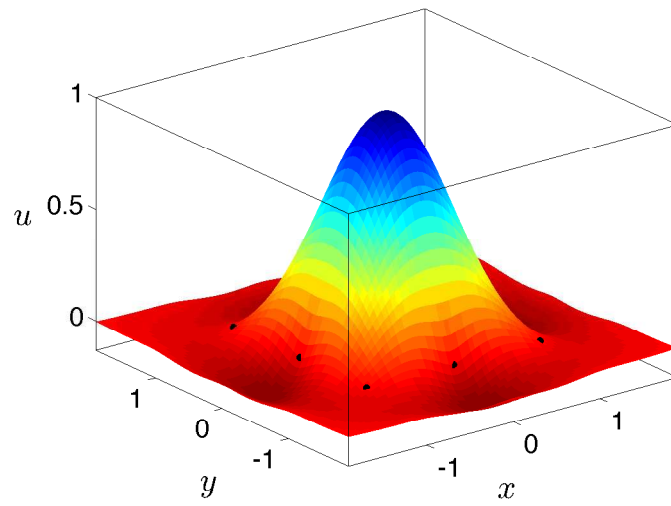
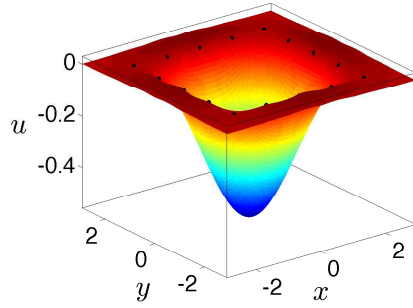
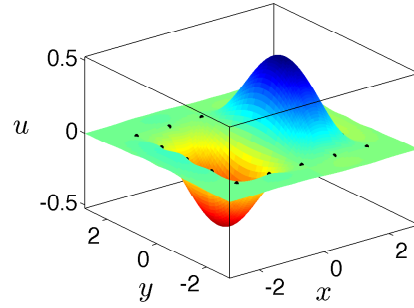


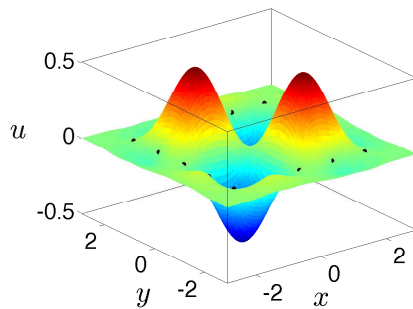
Figure 6: Mode shape ($\text{Re}\{u^{(d)}\}$) for a single defect in doubly periodic domain $a \simeq 2.53728$, $b/a = 1$.



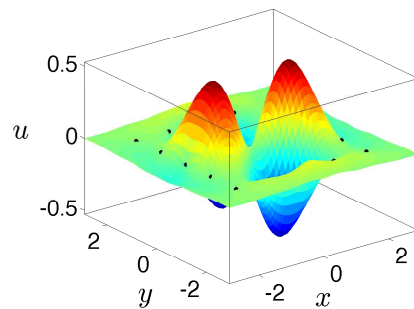
(a)



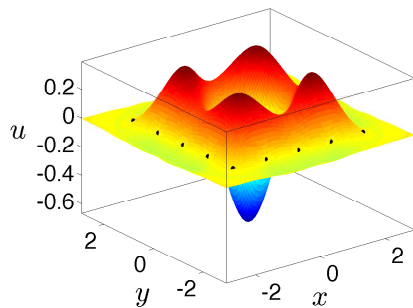
(b)



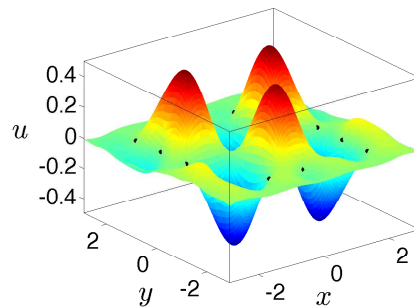
(c)



(d)

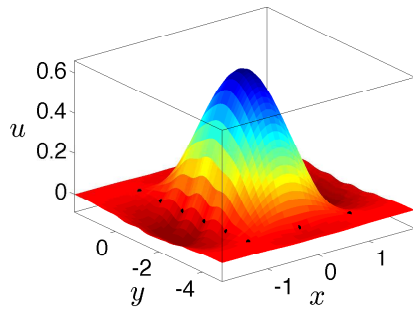


(e)

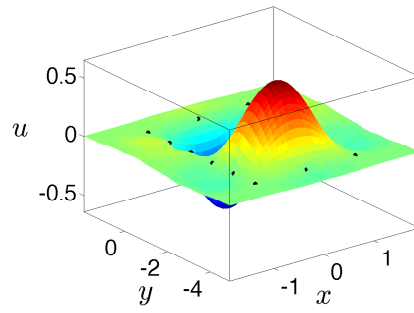


(f)

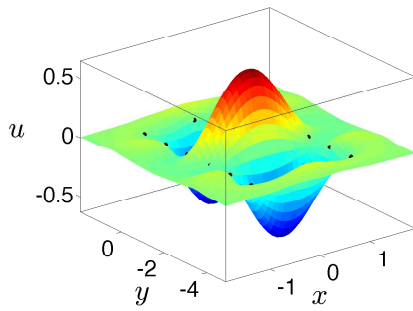
Figure 7: Mode shapes that are supported inside 3×3 defect in doubly periodic domain ($b/a = 1$) at (a): $a \simeq 1.35692$, (b): $a \simeq 1.95271$, (c): $a \simeq 2.38206$, (d): $a \simeq 2.61818$, (e): $a \simeq 2.62461$ and (f): $a \simeq 2.93110$.



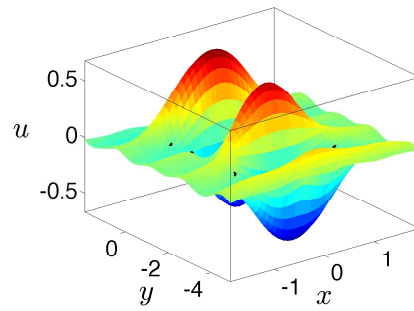
(a)



(b)

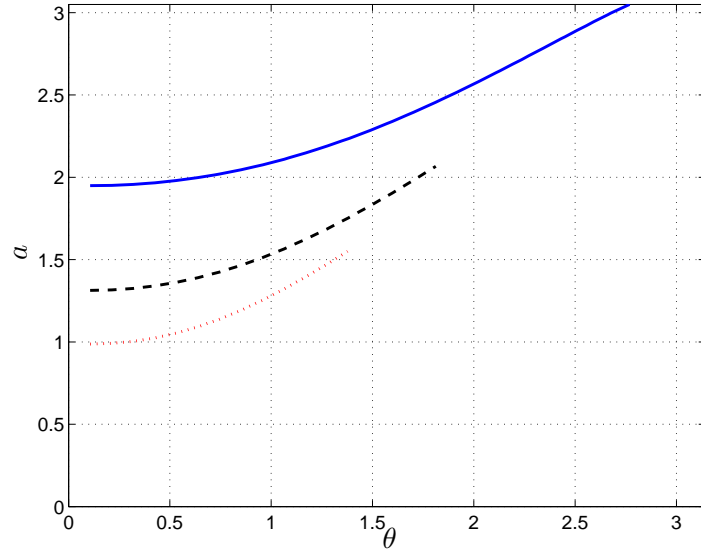


(c)

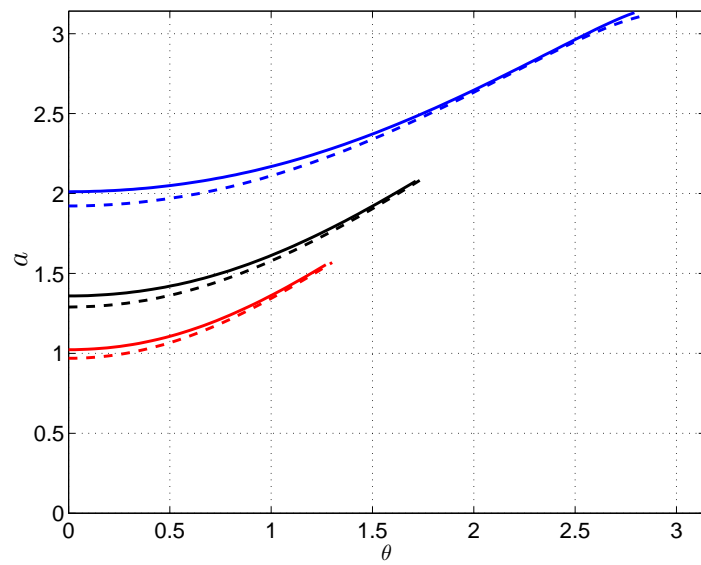


(d)

Figure 8: Mode shapes that are supported inside 4×1 defect (or 1×4 defect) in doubly periodic domain ($b/a = 1$) at (a): $a \simeq 2.04864$, (b): $a \simeq 2.28328$, (c): $a \simeq 2.63330$, and (d): $a \simeq 3.03234$.



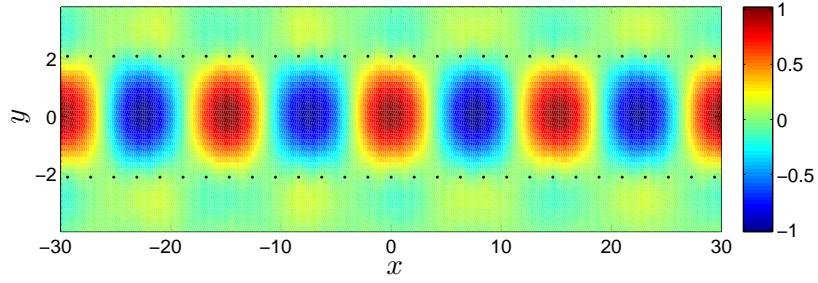
(a)



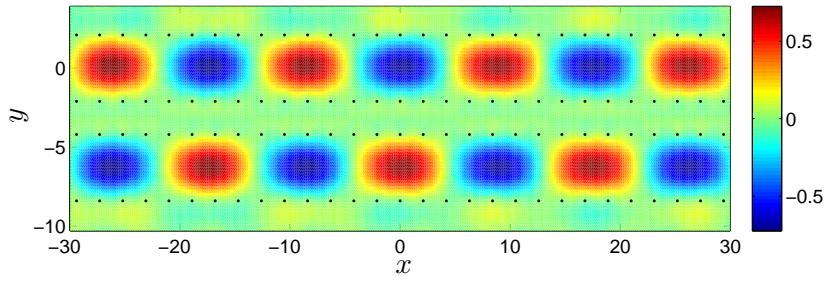
(b)

47

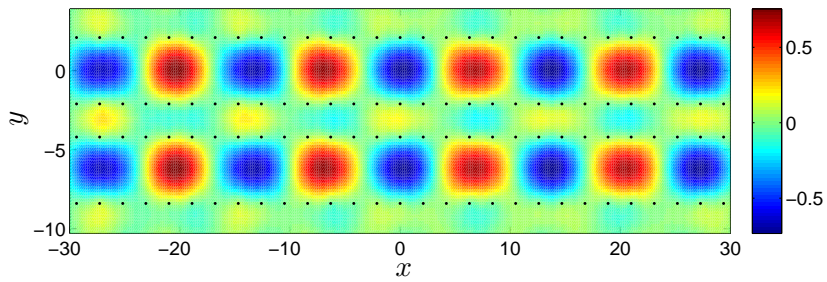
Figure 9: (a): Plot showing the values of a for which $\det\{K_{m,q}\} = 0$ for a single line defect ($m = 0$). (b): Values of a when $\det\{K_{m,q}\} = 0$ for the two line defect case ($m = 0, -3$) where $b/a = 1$ (blue curve), $b/a = 1.5$ (black curve), $b/a = 2$ (red curve).



(a)



(b)



(c)

Figure 10: (a): Waveguide mode ($\text{Re}\{u^{(d)}\}$) for a single line defect at $\theta = 0.87850$ for $a = 2.1$, $b/a = 1$. (b-c): Waveguide modes for a double line defect corresponding to (b) $\theta = 0.75567$ and (c) $\theta = 0.97115$ with $a = 2.1$ and $b/a = 1$.